Table 1 Error analysis[a,b] of present interpolation algorithm, Laplacian, and reciprocal distance weighted-averaging methods

Method[c]	Mesh[d]	$\sin(x+y)$	$\exp(x+y)$	$(x+y)^2$	$(x+y)$
1	1	−3.67	−1.36	−3.15	−5.90
2	1	−2.86	−0.54	−2.40	−6.66
3	1	−2.16	0.40	−1.08	−1.99
1	2	−3.68	−1.22	−3.21	−6.05
2	2	−2.94	−0.61	−2.49	−6.66
3	2	−2.38	0.003	−1.35	−2.25

[a]The present error analysis is performed on VAX 8600.

[b]The values of interpolation error are calculated by the expression $\log_{10}(\sqrt{\Sigma_i \Delta_i^2/Ne})$. In this mathematical expression, Ne indicates the number of cells and Δ_i represents the value of numerical difference between exact and interpolation results at centroid of cell i.

[c]The following three interpolation methods are used: 1) present interpolation algorithm, 2) Laplacian weighted-averaging method, and 3) reciprocal distance weighted-averaging method.

[d]The following two kinds of meshes are used: 1) Fig. 1a (1594 triangles and 472 quadrilaterals) and 2) Fig. 1b (1114 triangles and 1496 quadrilaterals).

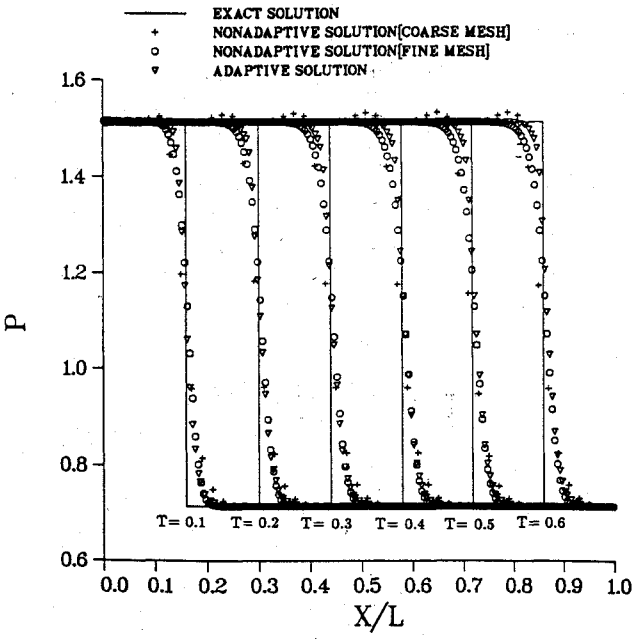

Fig. 3 Pressure distributions along the lower wall for the shock propagation in a channel.

times the CPU time required to run the flow solver on the coarse mesh. The CPU time required for the computation on the fine mesh, however, is about 3.5 times that required for the computation on the adaptive mesh. Based on the preceding discussion, the accuracy and efficiency of present solution-adaptive approach are confirmed.

Conclusions

To study the unsteady inviscid flow problems, a solution-adaptive approach has been presented in this paper. An adaptive mesh technique is developed on quadrilateral-triangular meshes and incorporated with the Euler solution procedure, that includes a locally implicit cell-centered finite volume TVD scheme[4] and the numerical treatments of boundary conditions. For the present adaptive mesh technique, an unstructured mesh generation method[2] is adopted. The magnitude of density gradient $|\nabla\rho|$ is chosen as the enrichment indicator. To reduce the CPU time and numerical error arising from the mesh coarsening and the interpolation of flow properties, a two-level refinement technique and an interpolation algorithm are created. From the error analysis for $\sin(x+y)$, $\exp(x+y)$, $(x+y)^2$, and $(x+y)$ functions, the present interpolation algorithm is accurate. For the shock propagation in a channel, the meshes can be properly refined in time according to the unsteady flow solutions. On the coarse, fine, and adapted meshes, respectively, the pressure distributions along the lower wall and CPU time required for those computations indicate that the present solution-adaptive approach is accurate, efficient, and reliable.

References

[1]Rausch, R. D., Batina, J. T., and Yang, H. T. Y., "Spatial Adaptation of Unstructured Meshes for Unsteady Aerodynamic Flow Computations," *AIAA Journal*, Vol. 30, No. 5, 1992, pp. 1243–1251.

[2]Hwang, C. J., and Wu, S. J., "Global and Local Remeshing Algorithms for Compressible Flows," *Journal of Computational Physics*, Vol. 102, No. 1, 1992, pp. 98–113.

[3]Webster, B. E., Shephard, M. S., Rusak, Z., and Flaherty, J. E., "Automated Adaptive Time-Discontinuous Finite Element Method for Unsteady Compressible Airfoil Aerodynamics," *AIAA Journal*, Vol. 32, No. 4, 1994, pp. 748–757.

[4]Hwang, C. J., and Yang, S. Y., "Locally Implicit Total Variation Diminishing Schemes on Mixed Quadrilateral-Triangular Meshes," *AIAA Journal*, Vol. 31, No. 11, 1993, pp. 2008–2015.

[5]Bockelie, M. J., and Eiseman, P. R., "A Time-Accurate Adaptive Grid Method and the Numerical Simulation of a Shock-Vortex Interaction," NASA TP-2998, March 1990.

[6]Nielson, G. M., and Franke, R., "Surface Construction Based Upon Triangulations," *Surfaces in CAGD*, edited by R. E. Barnhill and W. Boehm, North-Holland, Amsterdam, 1983, pp. 163–177.

[7]Hwang, C. J., and Fang, J. M., "Solution-Adaptive Approach for Unsteady Flow Calculations on Quadrilateral-Triangular Meshes," AIAA Paper 95-1723, June 1995.

Fluorescence Velocity Measurements in the Interior of a Hydrogen Arcjet Nozzle

P. Victor Storm* and Mark A. Cappelli†
Stanford University, Stanford, California 94305-3032

Introduction

As arcjet thrusters have advanced from laboratory devices to in-flight operational thrusters for satellite north-south station-keeping, there has been an increase in interest in improving arcjet efficiency and operating range. These improvements will be obtained primarily through advanced analytical modeling of arcjets; however, validation of the models can be performed only by comparison with experimental measurements of operating parameters and plasma properties. During the past several years, a number of optical diagnostics have been developed to investigate properties in the plasma plume of the arcjet. Primary among these diagnostics is laser-induced fluorescence (LIF), which has proven very useful because of its abundant signal level, very good spatial resolution, and specie-specific nature. Plasma properties in the plume of an arcjet thruster operating on a variety of propellants have been measured using LIF. Liebeskind et al.[1] measured atomic hydrogen translational temperature and velocity at the exit plane of a 1-kW hydrogen arcjet thruster, and investigated slip velocity by the fluorescence of helium in a helium-seeded hydrogen arcjet.[2] Ruyten and Keefer[3] measured velocity in an argon plume of a 0.3-kW arcjet, and Ruyten et al.[4] performed LIF on atomic hydrogen and nitrogen to measure velocity in a 1-kW arcjet plume using simulated ammonia as the propellant. Recently, Pobst et al.[5] measured ground-state atomic hydrogen density, temperature, and velocity profiles at the exit plane of a 1-kW hydrogen arcjet using pulsed two-photon LIF.

Although LIF has been successfully applied to arcjet thrusters as a plasma plume diagnostic, it has not been used previously to investigate plasma properties within the nozzle because of geometric constraints and reduced signal-to-background noise ratios. Optical studies of the plasma in the interior of the arcjet were performed

Received Aug. 14, 1995; revision received Oct. 25, 1995; accepted for publication Nov. 14, 1995.

*Research Assistant, High Temperature Gasdynamics Laboratory, Department of Mechanical Engineering. Student Member AIAA.

†Associate Professor, High Temperature Gasdynamics Laboratory, Department of Mechanical Engineering. Member AIAA.

previously only in emission.[6] An analysis based on collisional-radiative modeling suggests the feasibility of applying laser-induced fluorescence to the plasma in the interior of a low-power hydrogen arcjet.[7] The first use of laser-induced fluorescence for spatially resolved plasma velocity measurements within an arcjet nozzle are described. The arcjet was operated on a propellant of pure hydrogen. The Balmer-α transition of atomic hydrogen was scanned by the excitation laser source while simultaneously detecting the spectrally integrated resonance fluorescence. Velocity was determined from the Doppler shift in the peak of the laser excitation spectrum relative to a stationary reference. The arcjet operating conditions were chosen to facilitate a comparison between these measurements and arcjet modeling results of Butler et al.[8,9]

Experiment

The arcjet thruster used in this experiment was a 1-kW-class radiatively cooled laboratory-type thruster. The tungsten nozzle (Fig. 1) consisted of a 0.635-mm-diam, 0.25-mm-long throat and a 12.1-mm-long conical diverging section at a half angle of 20 deg. With a design area ratio of 225, the exit plane diameter was 9.53 mm. The tip of the 2% thoriated tungsten cathode was originally set approximately 0.45 mm upstream of the nozzle constrictor; however, with erosion of the cathode, this value may be somewhat larger. The arcjet was operated at a current and voltage of 9.8 ± 0.1 A and 151 ± 1 V, respectively, and a fixed H_2 mass flow rate of 14.2 mg/s. The vacuum facility consisted of a 1.09×0.56 m diam stainless-steel chamber, that was maintained at background pressure of approximately 0.35 torr by two 590-l/s blowers.

The fluorescence excitation was provided by a continuous-wave ring dye laser pumped by an argon-ion laser. The dye laser was operated with DCM dye that has a broad emission band centered around 650 nm, making this dye particularly suitable for the Balmer-α excitation of hydrogen at 656.28 nm. Dye laser output up to 200 mW was obtained with a pump laser power of 4 W. Scanning of the ring dye laser across the Balmer-α transition was performed with a tunable, piezoelectrically driven intracavity etalon. The scanning range was limited by laser mode instability to approximately 50 GHz, or 0.075 nm, which was on the order of the linewidth of the Balmer-α line at the conditions in the nozzle. The laser beam was directed axially into the plasma to probe the interior of the arcjet and to use the nozzle as a beam dump. Consequently, the axial-velocity component was measured from the Doppler shift of the line. The fluorescence was collected through a window on the vacuum chamber end plate at an angle of 16 deg from the arcjet axis, and detected broadband with a photomultiplier tube. The spatial resolution was approximately 0.6 mm in the axial direction and 30 μm in the transverse directions, as determined by the laser beam waist and the collection optics. The spectral resolution of the laser was 4×10^{-4} nm. By translating the arcjet axially and radially, velocity measurements were obtained along the arcjet centerline as well as radially at a few axial positions, as indicated by the crosshatches in Fig. 1. A fraction of the excitation laser beam from the dye laser was split off and sent to a photodiode detector and a wavemeter to monitor the laser intensity and wavelength. The fluorescence signal was normalized by the laser intensity, but was not corrected for possible fluctuations in laser wavelength, which were believed to be negligible.

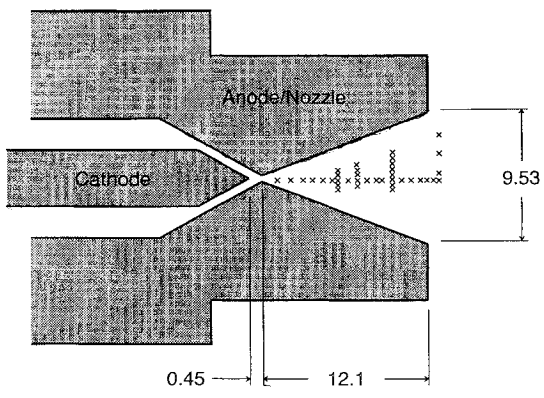

Fig. 1 Schematic cross section of the 1-kW arcjet thruster nozzle (not to scale). All dimensions are in millimeters. Crosshatches indicate the positions where the measurements were taken.

Since the fluorescence signal was considerably smaller than the background emission, phase-sensitive detection was performed by mechanically chopping the excitation beam at a frequency of 1.5 kHz and detecting the signal with a digital lock-in amplifier. Noise at the chopping frequency, due mainly to scattered laser light in the arcjet, was the primary limitation in obtaining a significant signal in regions of weak fluorescence. Velocity measurements were taken from the nozzle exit plane to within 1.5 mm of the throat, at which point the LIF signal was overwhelmed by the background of scattered laser light.

Analysis

The recorded fluorescence signal was normalized by the photodiode output to account for variations in the laser power during the scanning of the spectral line. The wavelength was obtained from the wavemeter, an instrument that determines absolute wavelength by the interference of the input laser signal with an internal reference. The Doppler shift of the line center was accurately determined by fitting the normalized line shape with a Gaussian profile. The Balmer-α transition of atomic hydrogen is an electronic transition between the first and second excited states, i.e., $n = 2 \rightarrow n = 3$. This transition comprises five fine-structure components formed because of spin-orbit coupling; however, because the fine-structure splitting was considerably smaller than the line broadening at the conditions encountered in the arcjet plasma, it was therefore neglected. Although non-Gaussian broadening mechanisms of the spectral line, such as Stark broadening, were believed to be present and comparable with the Doppler broadening, a simple Gaussian fit was sufficient to determine the spectral line center. A Voigt fit was unnecessary and less accurate, given the scarcity of data in the line wings. Since the scanning was performed on the laser excitation and not on the fluorescence collection, the Doppler shift is only associated with the component of the velocity in the direction of the laser excitation, namely, in the direction parallel to the nozzle axis. This axial velocity component u_z was determined from the shift of the spectral line center Δv from a stationary reference frequency v_0 according to

$$u_z/c = \Delta v/v_0$$

The stationary reference was obtained from previous LIF measurements performed on the same arcjet at the same facility by Liebeskind et al.[1] The pressure shift of the spectral line is negligible in comparison with the Doppler shift.

Results and Conclusions

Measurements of axial velocities along the nozzle centerline and along three diameters are given in Figs. 2 and 3, respectively. The axial position is defined as zero at the exit plane and negative into the nozzle. Hence, the nozzle throat is located at -12.1 mm. The centerline velocity drops monotonically from a peak of approximately 17.5 km/s at 1.3 mm downstream of the throat to around 12 km/s at the exit plane. Since no other measurements of velocity have been made within the arcjet nozzle, the results can only be compared to the modeling work of Butler et al.[8] The results of two versions of this model are shown in Fig. 2. One version includes mass diffusion terms in the species momentum equation, whereas the other does not include such terms. There is remarkably good agreement between the measurements and the former model, clearly indicating the importance of including diffusional processes to correctly model the transport of heavy species in the plasma. This is not surprising considering the large radial gradients in plasma properties within the nozzle.[9] The only significant discrepancy between the model results and measurements are in the three data points closest to the throat of the arcjet. However, in this region the measurements have the largest uncertainty because of the reduced LIF signal and the increased background noise.

Figure 3 displays radial profiles of the axial velocity measured at three axial positions within the nozzle (2.54, 5.08, and 6.35 mm

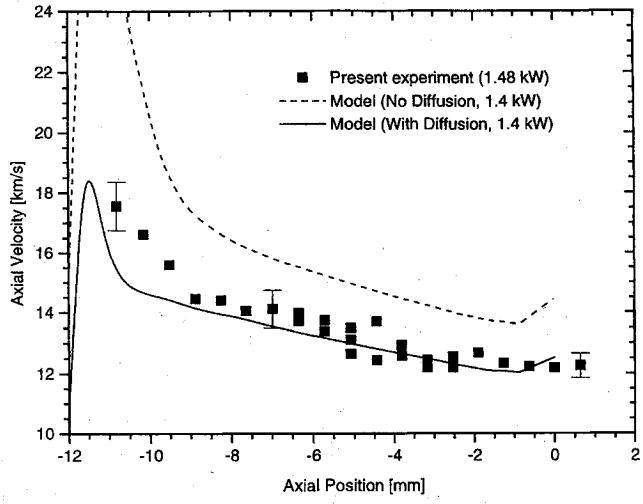

Fig. 2 Measured axial velocity along the arcjet centerline. Typical errors are shown. The measurements are compared to results of an arcjet model incorporating mass diffusion and without mass diffusion.

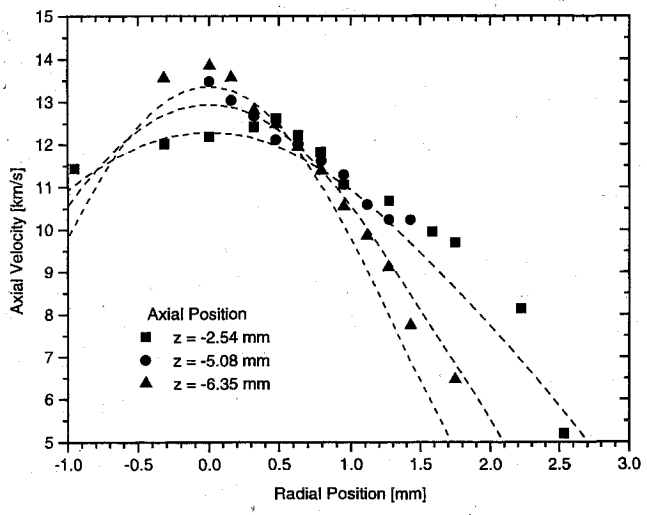

Fig. 3 Radial profiles of axial velocity at three axial locations within the arcjet nozzle. Errors are typically ±0.6 km/s. The dashed lines are results of the arcjet model (with diffusion) at the same axial locations as the measurements.

upstream from the exit plane). The LIF signal intensity dropped off quickly with radial position, indicating a rapid radial decrease in the $n = 2$ excited-state number density of atomic hydrogen. This loss in signal restricted the measurement domain to within approximately 2 mm of the nozzle centerline. The dashed lines in the figure are the model results at the same axial locations as the measurements. The measurements and the model show remarkably good agreement; however, the measured velocities are somewhat greater than those of the model away from the arcjet centerline. Although the centerline velocity decreases axially, the velocities away from the centerline increase with axially position. Because most of the mass convection occurs in this outer region, the total kinetic energy of the flow is clearly increasing downstream, as is expected in a supersonic diverging nozzle.

At present, experiments are under way to perform a more comprehensive study to map the velocity flowfield at various arcjet specific energies for both hydrogen and simulated hydrazine propellants.

Acknowledgments

This work was supported in part by the U.S. Air Force Office of Scientific Research and Olin Aerospace Company. Special acknowledgments are given to NASA Lewis Research Center for supplying the arcjet thruster and power supply and to G. W. Butler of Olin-Aerospace Company for providing the arcjet modeling results.

References

[1]Liebeskind, J. G., Hanson, R. K., and Cappelli, M. A., "Laser-Induced Fluorescence Diagnostic for Temperature and Velocity Measurements in a Hydrogen Arcjet Plume," *Journal of Applied Optics*, Vol. 32, No. 30, 1993, pp. 6117–6127.

[2]Liebeskind, J. G., Hanson, R. K., and Cappelli, M. A., "Experimental Investigation of Velocity Slip Near an Arcjet Exit Plane," *AIAA Journal*, Vol. 33, No. 2, 1994, pp. 373–375.

[3]Ruyten, W. M., and Keefer, D., "Characterization of Electric Thruster Plumes Using Multiplexed Laser-Induced Fluorescence Measurements," AIAA Paper 92-2965, July 1992.

[4]Ruyten, W. M., Burtner, D., and Keefer, D., "Laser-Induced Fluorescence Measurements on the Plume of a 1 kW Arcjet Operated on Simulated Ammonia," International Electric Propulsion Conf., Seattle, WA, Paper 93-127, Sept. 1993.

[5]Pobst, J. A., Wysong, I. J., and Spores, R. A., "Laser Induced Fluorescence of Ground State Hydrogen Atoms at Nozzle Exit of an Arcjet Thruster," AIAA Paper 95-1973, June 1995.

[6]Cappelli, M. A., and Storm, P. V., "Interior Plasma Diagnostics of Arcjet Thrusters," AIAA Paper 94-2654, June 1994.

[7]Storm, P. V., and Cappelli, M. A., "Laser-Induced Fluorescence Measurements Within an Arcjet Thruster Nozzle," AIAA Paper 95-2381, July 1995.

[8]Butler, G. W., Kashiwa, B. A., and King, D. Q., "Numerical Modeling of Arcjet Performance," AIAA Paper 90-1474, June 1990.

[9]Butler, G. W., Boyd, I. D., and Cappelli, M. A., "Nonequilibrium Flow Phenomena in Low-Power Hydrogen Arcjets," AIAA Paper 95-2819, July 1995.

Shape and Placement of Piezoelectric Sensors for Panel Flutter Limit-Cycle Suppression

Zhihong Lai,* Jen-Kuang Huang,† and Chuh Mei‡
Old Dominion University,
Norfolk, Virginia 23529-0247

Introduction

It is well known that the electrode pattern of piezoelectric materials can be shaped to produce beneficial response of sensors and actuators. Lee and Moon[1] showed that shaped piezoelectric layers can be used as modal sensors and actuators that only sense or actuate certain modes. On the other hand, panel flutter has been encountered in the operation of aircraft and missiles at transonic and supersonic speeds. It is a large-deflection limit-cycle oscillation excited by the airflow[2] that is only on one side of the panel. Lai et al.[3] demonstrated the panel flutter limit-cycle suppression by using piezoelectric actuation with active control. The flutter free region can be enlarged by using the piezoelectric actuation.

In this paper, a method to design sensors (position and rate sensor) for panel flutter suppression is presented. The shape and location of sensors are based on the control feedback gain. The optimal control performance can be achieved by using these sensors with a constant gain direct feedback controller. Numerical simulation is demonstrated for panel flutter suppression by using the shaped sensors designed with this novel approach.

Sensor Design

For curvature sensing, two sensor layers that are placed symmetrically to the midplane are composed as a sensor unit, which is

Received March 2, 1995; revision received June 12, 1995; accepted for publication June 19, 1995.

*Research Associate, Department of Mechanical Engineering.

†Associate Professor, Department of Mechanical Engineering. Senior Member AIAA.

‡Professor, Department of Aerospace Engineering. Associate Fellow AIAA.